# Biochemical and biological properties of cortexillin III, a component of *Dictyostelium* DGAP1–cortexillin complexes

Xiong Liu[a,*], Shi Shu[a,*], Shuhua Yu[a], Duck-Yeon Lee[b], Grzegorz Piszczek[c], Marjan Gucek[d], Guanghui Wang[d], and Edward D. Korn[a]

[a]Laboratory of Cell Biology, [b]Biochemistry Core, [c]Biophysics Core, and [d]Proteomics Core, National Heart, Lung, and Blood Institute, National Institutes of Health, Bethesda, MD 20892

**ABSTRACT** **Cortexillins I–III are members of the α-actinin/spectrin subfamily of *Dictyostelium* calponin homology proteins. Unlike recombinant cortexillins I and II, which form homodimers as well as heterodimers in vitro, we find that recombinant cortexillin III is an unstable monomer but forms more stable heterodimers when coexpressed in *Escherichia coli* with cortexillin I or II. Expressed cortexillin III also forms heterodimers with both cortexillin I and II in vivo, and the heterodimers complex in vivo with DGAP1, a *Dictyostelium* GAP protein. Binding of cortexillin III to DGAP1 requires the presence of either cortexillin I or II; that is, cortexillin III binds to DGAP1 only as a heterodimer, and the heterodimers form in vivo in the absence of DGAP1. Expressed cortexillin III colocalizes with cortexillins I and II in the cortex of vegetative amoebae, the leading edge of motile cells, and the cleavage furrow of dividing cells. Colocalization of cortexillin III and F-actin may require the heterodimer/DGAP1 complex. Functionally, cortexillin III may be a negative regulator of cell growth, cytokinesis, pinocytosis, and phagocytosis, as all are enhanced in cortexillin III–null cells.**

**Monitoring Editor**
Peter Van Haastert
University of Groningen

Received: Aug 9, 2013
Revised: Apr 16, 2014
Accepted: Apr 29, 2014

## INTRODUCTION

The *Dictyostelium discoideum* genome includes 36 calponin homology (CH) domain proteins (Friedberg and Rivero, 2010), defined as proteins with sequences homologous to repeating sequences in the N-terminal ~100 amino acids of the regulatory smooth muscle protein calponin (Castresana and Saraste, 1995). Of these 36 proteins, 14 comprise the α-actinin/spectrin family of proteins with dual CH domains (Friedberg and Rivero, 2010). This family includes the extensively studied actin-binding proteins filamin and α-actinin, the less-studied actin cross-linking proteins cortexillin (ctx) I and II, and the recently identified ctxIII (Lee *et al.*, 2010), about which very little is known.

The amino acid sequences of ctxI (444 residues, $M_r$ = 50,505) and ctxII (441 residues, $M_r$ = 50,460) are 60% identical, and the C-termini of ctxI and ctxII have heptad repeats predicted to form coiled-coils (Faix *et al.*, 1996; Steinmetz *et al.*, 1998). As predicted from its sequence, recombinant ctxI forms parallel homodimers with N-terminal dual globular heads, which contain the CH-domain actin-binding sites, and a coiled-coil C-terminal domain (Faix *et al.*, 1996). The C-terminus of ctxI, but not of ctxII, also contains a phosphatidylinositol (4,5)-bisphosphate ($PIP_2$)–binding site and a second, and stronger, actin-bundling site that is inhibited by $PIP_2$ (Stock *et al.*, 1999).

In vitro, ctxI binds to the *Dictyostelium* GAP proteins DGAP1 (associated gene rgaA) and GAPA (associated gene gapA) through its C-terminal domain (Faix *et al.*, 2001). DGAP1 and GAPA have also been called IQGAP1 and IQGAP2 because of their sequence similarities to the C-terminal halves of yeast and human IQGAPs (Shannon, 2012), but we prefer DGAP1 and GAPA because neither protein contains the canonical IQ domain present in yeast and human IQGAPs (Shannon, 2012). In experiments with cell lysates, DGAP1 and GAPA were found to bind to both Rac1A and ctxI (Faix *et al.*, 2001), forming ternary complexes, and also to ctxII, which raises the possibility that there may be quaternary, as well as ternary,

This article was published online ahead of print in MBoC in Press (http://www.molbiolcell.org/cgi/doi/10.1091/mbc.E13-08-0457) on May 7, 2014.

*These authors contributed equally.

Address correspondence to: Edward D. Korn (edk@nih.gov).

Abbreviations used: CH, calponin homology; ctx, cortexillin; MS, mass spectrometry.

complexes (Faix *et al.*, 2001). Because ctxII has been reported not to bind to either DGAP1 or GAPA in the absence of ctxI (Faix *et al.*, 2001), a quaternary complex would likely involve a heterodimer of ctxI and ctxII (Faix *et al.*, 2001).

In vivo, complexes of ctxI, ctxII, Rac1, and DGAP1 or GAPA (Faix *et al.*, 2001; Lee *et al.*, 2010; Mondal *et al.*, 2010) occur in the cortex (hence the name cortexillin) of vegetative amoebae and in the cortical region of spreading cells (where, together with myosin II, they appear to cross-link actin filaments in antiparallel bundles; Schroth-Diez *et al.*, 2009), in the leading edge (and to a lesser extent the rear) of motile cells, and in the cleavage furrow of dividing cells (Faix *et al.*, 1996). Elimination of both isoforms, but principally ctxI, results in flattened, multinucleate cells (Faix *et al.*, 1996). Ctxl$^{-}$II$^{-}$ cells have decreased cortical tension (Simson *et al.*, 1998), and the cortexillins, together with myosin II, generate equatorial forces in cytokinesis (Girard *et al.*, 2004). Lee *et al.* (2010) showed that disruption of the cortexillin complexes results in overextended activation of phosphoinositide 3-kinase and protein kinase B activity in response to cAMP signaling. We reported (Shu *et al.*, 2012) that double knockout of ctxI and ctxII inhibits all intracellular and extracellular responses to extracellular cAMP stimulation, possibly as a result of the altered cytoskeleton of these cells. Consequently, cAMP-induced cell streaming and development beyond the mound stage are completely blocked in ctxI$^{-}$II$^{-}$ cells (Shu *et al.*, 2012).

The cellular localizations of ctxI and ctxII and the phenotypes of ctxI$^{-}$, ctxII$^{-}$, and ctxI$^{-}$II$^{-}$ cells support the conclusion that ctxI and ctxII, together with myosin II, are required for maintaining a properly organized actin cytoskeleton (Schroth-Diez *et al.*, 2009; Shu *et al.*, 2012), increasing cleavage furrow stiffness (Girard *et al.*, 2004; Reichl *et al.*, 2008), cytokinesis (Faix *et al.*, 1996; Weber *et al.*, 1999), and fully functional cAMP-induced chemotaxis (Lee *et al.*, 2010; Shu *et al.*, 2012). CtxI and myosin II are also proposed to serve as a mechanosensor (Kee *et al.*, 2012), and both ctxI and ctxII are essential components of the mechanotransduction system in *Dictyostelium* (Effler *et al.*, 2006; Ren *et al.*, 2009; Dickinson *et al.*, 2012; Kee *et al.*, 2012).

In a study of the roles of DGAP1, GAPA, ctxI, and ctxII in signaling events at the leading edge of chemotaxing cells, Lee *et al.* (2010) serendipitously observed that, in addition to three Rac 1 isoforms, ctxI, and ctxII, a previously undescribed protein coimmunoprecipitated with DGAP1 but not with GAPA. Because of its sequence similarity to ctxI and ctxII (Friedberg and Rivero, 2010), Lee *et al.* (2010) named this protein (DDB0232236) ctxIII ($M_r$ = 55,659). Lee *et al.* (2010) further reported that ctxIII$^{-}$ cells had a 50% reduction in velocity and a decrease in directionality of cell motility in response to cAMP-stimulation. In this article, we report the results of the first study of the properties of recombinant ctxIII, the composition of a purified biological complex containing ctxIII, and the phenotype of ctxIII$^{-}$ cells.

## RESULTS

### Properties of recombinant cortexillin III in vitro

The sequence of ctxIII is 44% identical to the sequences of ctxI and ctxII, and the C-terminal regions of all three cortexillins contain sequences predicting coiled-coil formation, with, however, an appreciably lower probability for ctxIII than for ctxI and ctxII (Figure 1A). To determine whether ctxIII forms homodimers, we expressed FLAG-ctxIII in SF9 cells. To determine whether ctxIII forms heterodimers with ctxI and ctxII, we coexpressed FLAG-ctxIII with histidine (His)-ctxI and with His-ctxII (which were also expressed individually) in *Escherichia coli*. The recombinant proteins were purified by chromatography on a FLAG-affinity column, a Ni-nitriloacetic acid (NTA) column, or sequentially on both columns, as appropriate.

When analyzed by SDS–PAGE, the singly expressed proteins showed only one band (Figure 1B) and the doubly expressed proteins two bands of equivalent intensities (Figure 1, C and D), indicative that ctxIII can form heterodimers with both ctxI and ctxII. Analytical ultracentrifugation showed that both recombinant ctxI and ctxII (Figure 1, E and F) formed homodimers that accounted for 95 and 90%, respectively, of the total protein (Table 1), as previously shown for ctxI (Faix *et al.*, 1996). However, the major peak of recombinant ctxIII (Figure 1G) was monomeric, accounting for 52% of the total protein (Table 1), with the remainder being a mixture of unidentified, higher-order aggregates with $S > 5$ (Figure 1G). The lesser dimerization of ctxIII compared with ctxI and II is consistent with the lower probability of the C-terminal region of ctxIII to form coiled-coils (Figure 1A). Coexpressed ctxIII and ctxI and coexpressed ctxIII and ctxII formed heterodimers (Figure 1, H and I), accounting for 60 and 70%, respectively, of the total protein (Table 1) with higher oligomers also present. Presumably the ability of ctxIII to form heterodimers, when it does not form stable homodimers, is driven by the higher probability of ctxI and ctxII to form coiled coils.

None of the recombinant proteins had any effect on either the rate or extent of actin polymerization (Figure 2A). Recombinant ctxI homodimer bound to F-actin (Figure 2B) with $K_d \approx 0.2$ μM, very similar to that observed by Faix *et al.* (1996), calculated in both cases assuming independent binding of the two components in the homodimer. At saturation, we found that one ctxI homodimer bound to approximately four actin subunits, which also agrees with Faix *et al.* (1996). Recombinant ctxII homodimer bound to F-actin with significantly lower affinity than ctxI (Figure 2B), and ctxIII monomer (even if corrected for its relative impurity) bound to F-actin much more weakly than both ctxI and ctxII (Figure 2B). The recombinant heterodimers of ctxIII+II and ctxIII+I also bound weakly to F-actin, with substantially lower affinities than the homodimers of ctxI and ctxII (Figure 2B). The relatively strong affinity of ctxI for F-actin may be the consequence of the second actin binding in its C-terminus, which, by sequence comparison, is not present in either ctxII or ctxIII.

### Cell localization of expressed cortexillin III

FLAG-ctxIII expressed in wild-type (WT) cells colocalized with ctxI, ctxII, and F-actin in the cortex of vegetative cells (Figure 3A, top and bottom), further justifying the name cortexillin III, which was originally based on its sequence similarity to ctxI and ctxII (Lee *et al.*, 2010). As shown previously for ctxI and ctxII (Faix *et al.*, 1996), FLAG-ctxIII localized with F-actin at the leading edge (and less strongly at the rear) of starved motile cells (Figure 3B, top) and in the cleavage furrow of dividing cells (Figure 3B, bottom). In cells treated with latrunculin A to depolymerize actin filaments, both FLAG-ctxIII and actin were diffuse (Figure 3C, bottom), demonstrating that the localization of ctxIII in the cortex, like the localization of ctxI and II, requires filamentous actin.

Endogenous ctxI and ctxII localized to the cortex and cleavage furrow of dividing ctxIII$^{-}$ cells (Figure 3D), as they do in WT cells (Faix *et al.*, 1996). Although expressed green fluorescent protein (GFP)–ctxIII localized to the cortex of vegetative ctxI$^{-}$, ctxII$^{-}$, and ctxIII$^{-}$ cells (Figure 3E, top) and to the cleavage furrow of dividing ctxI$^{-}$, ctxII$^{-}$, and ctxII$^{-}$ cells (Figure 3E, bottom), GFP-ctxIII was diffuse when expressed in vegetative ctxI$^{-}$II$^{-}$ cells and did not localize to the cleavage furrow of dividing ctxI$^{-}$II$^{-}$ cells (Figure 3E, top and bottom). Thus the localization of ctxIII requires the presence of either ctxI or ctxII, whereas the localizations of ctxI and ctxII are

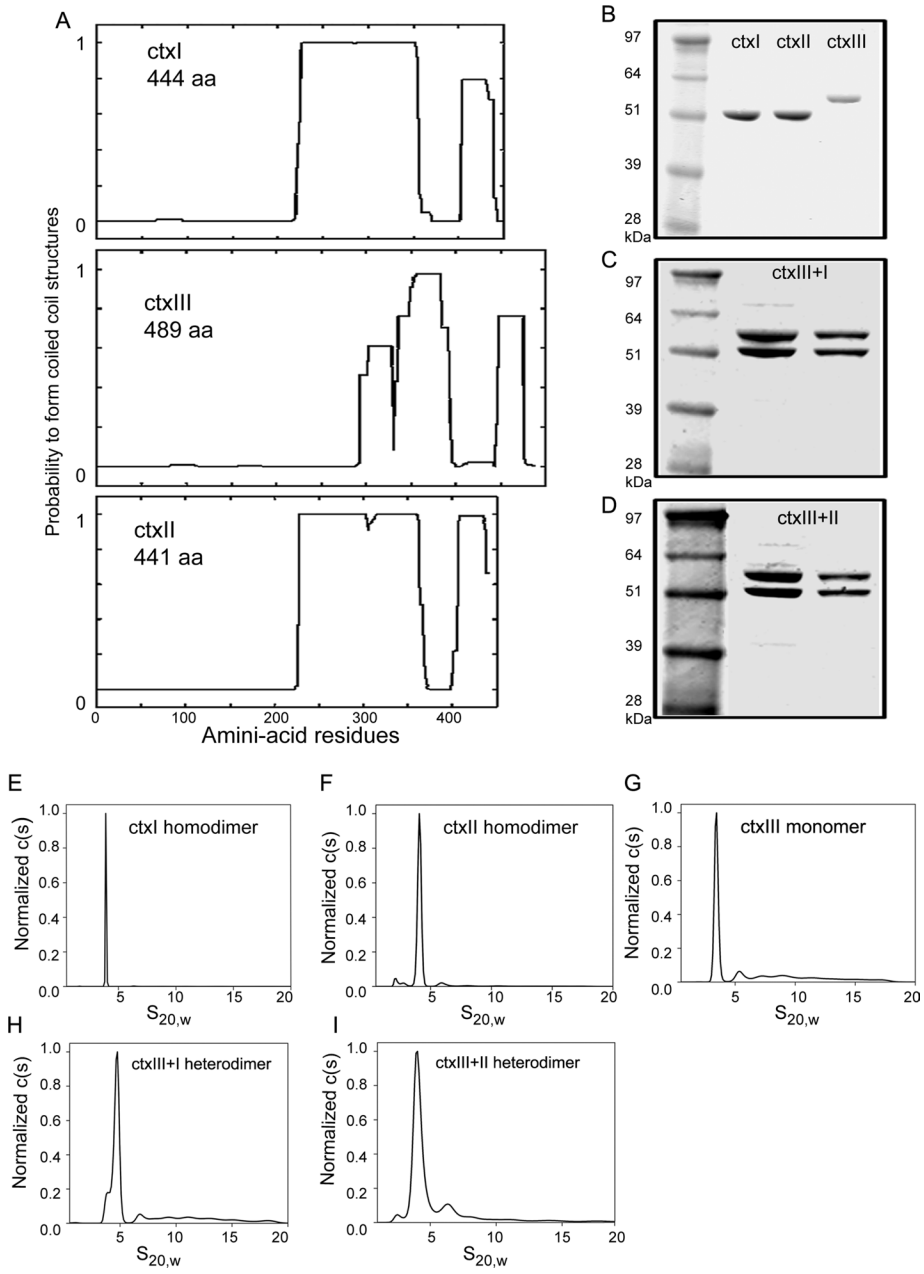


FIGURE 1: Recombinant ctxIII forms heterodimers with ctxI and ctxII. (A) Comparison of sequences of ctxI, ctxII, and ctxIII showing the probability of coiled-coil formation using matrix MTIDK and window width 28 (Lupas *et al*., 1991). (B–D) SDS–PAGE of (B) purified recombinant His-ctxI, His-ctxII, and FLAG-ctxIII; (C) purified recombinant ctxIII+I; and (D) purified recombinant ctxIII+II. The heterodimers in C and D were purified by sequential chromatography on a FLAG-affinity column (middle lane), followed by a Ni-NTA-affinity column (right lane). Upper bands are FLAG-ctxIII and lower bands are His-ctxI or His-ctxII. (E–I) Analytical ultracentrifugation of purified ctxI, ctxII, ctxIII, ctxIII+I, and ctxIII+II in 50 mM Tris-HCl, pH 7.4, and 300 mM NaCl. CtxI and ctxII were homodimers, ctxIII was mostly monomer, and the major peaks in ctxIII+I and ctxIII+II were heterodimers (Table 1).

independent of ctxIII (Figure 3D). Furthermore, GFP-ctxIII expressed in DGAP1$^-$ cells was mostly diffuse in the cytoplasm and did not localize to the cleavage furrow (Figure 3E).

### Proteins that coimmunoprecipitate with cortexillin III expressed in vivo

N-terminal GFP- and FLAG-ctxIII were expressed in ctxIII$^-$ cells, immunoprecipitated from lysates with magnetic beads coated with antibodies to the respective epitope tags, and the immunoprecipitates analyzed by SDS–PAGE (Figure 4, A–D). The immunoprecipitates of lysates of ctxIII$^-$ cells expressing GFP-ctxIII had three major bands, G1, G2, and G3, which were not present in immunoprecipitates of control cells expressing GFP (Figure 4A). The components of the three bands were identified by tandem mass spectrometry (MS/MS) of tryptic peptides (Table 2) as DGAP1 (band G1), GFP-ctxIII (band G2), and a mixture of ctxI and ctxII (band G3). Of note, the immunoprecipitate did not contain GAPA, consistent with the results of Lee *et al*. (2010) that immunoprecipitates of DGAP1 contain ctxIII but immunoprecipitates of GAPA do not.

Similarly, DGAP1, FLAG-ctxIII, ctxI, and ctxII were present in the major bands, F1, F2, and F3, respectively, of SDS–PAGE gels of immunoprecipitates of cells expressing FLAG-ctxIII (Figure 4B and Table 2). The presence of DGAP1, ctxI, and ctxII in the FLAG-immunoprecipitate was confirmed by Western blots (Figure 4, C and D). However, MS/MS analysis (Table 2) identified a second protein, cell division cycle protein D (cdcD), in band F1 of the FLAG-ctxIII immunoprecipitate that was not present in the corresponding band, G1, of the GFP-ctxIII immunoprecipitate. cdcD is an AAA-ATPase homologous to mammalian and yeast cdc48. Because cdcD was also present in the FLAG immunoprecipitate of control ctxIII$^-$ cells expressing FLAG-GFP (band C1 in Figure 4B and Table 2) and was not present in the GFP-immunoprecipitates (band G1 in Figure 4A and Table 2), cdcD must have bound nonspecifically to the anti-FLAG magnetic beads and not to FLAG-ctxIII. Of note, none of the gels showed any indication of Rac1 in the immunoprecipitates.

### Characterization of in vivo complexes of cortexillin III

To characterize further the putative complexes between ctxIII, ctxI, ctxII, and DGAP1, we chromatographed a lysate from cells expressing FLAG-ctxIII on a FLAG-affinity column composed of the same anti-FLAG antibody as on the anti-FLAG magnetic beads. SDS–PAGE of the proteins eluted from the column by FLAG-peptide contained the same three bands (Figure 4E, inset) that were identified in the immunoprecipitation by anti-FLAG magnetic beads (Figure 4B). Of importance, only one major peak was observed when the FLAG-peptide eluate was chromatographed on an HPLC gel filtration column (Figure 4E). Reverse-phase chromatography separated the single HPLC peak into four separate peaks (Figure 4F, top). As determined by MS (Figure 4F, bottom), peak 1 contained ctxI, peak 2 contained ctxII, peak 3 contained FLAG-ctxIII and cdcD, and peak 4 contained DGAP1. Thus

| Protein | Major peak (%) | $S_{20,w}$ (S) | $f/f_0$ | Expected mass[a] (kDa) | Monomer (M)/dimer (D) |
|---|---|---|---|---|---|
| His-ctx I | 95 | 3.9 | 2.0 | 105 | D |
| His-ctx II | 90 | 4.1 | 1.8 | 91 | D |
| FLAG-ctx III | 52 | 3.4 | 1.4 | 47 | M |
| FLAG-ctx III + His-ctxI | 60 | 4.7 | 1.6 | 91 | D |
| FLAG-ctx III + His-ctxII | 70 | 4.2 | 1.7 | 88 | D |

The monomeric masses from the sequences are His-ctxI, 52.5 kDa; His-ctxII, 52.4 kDa; and FLAG-ctxIII, 57.5 kDa. $f/f_0$ is the best-fit weight-average frictional ratio.
[a]Molecular mass of the major peak species calculated from the Svedberg relationship using fitted $f/f_0$ values and the hydrodynamic scaling law to obtain the molecular diffusion rate (Schuck, 2000). Typical accuracy of molecular mass calculations from sedimentation velocity data are within 10% of the expected value for distributions with a single dominant peak (Schuck, 2005). Because the frictional ratio is a weight average for all species in the distribution, the error of this calculation can increase when the major peak represents <90–95% of all species present.

TABLE 1: Analysis of analytical ultracentrifugation sedimentation velocity data.

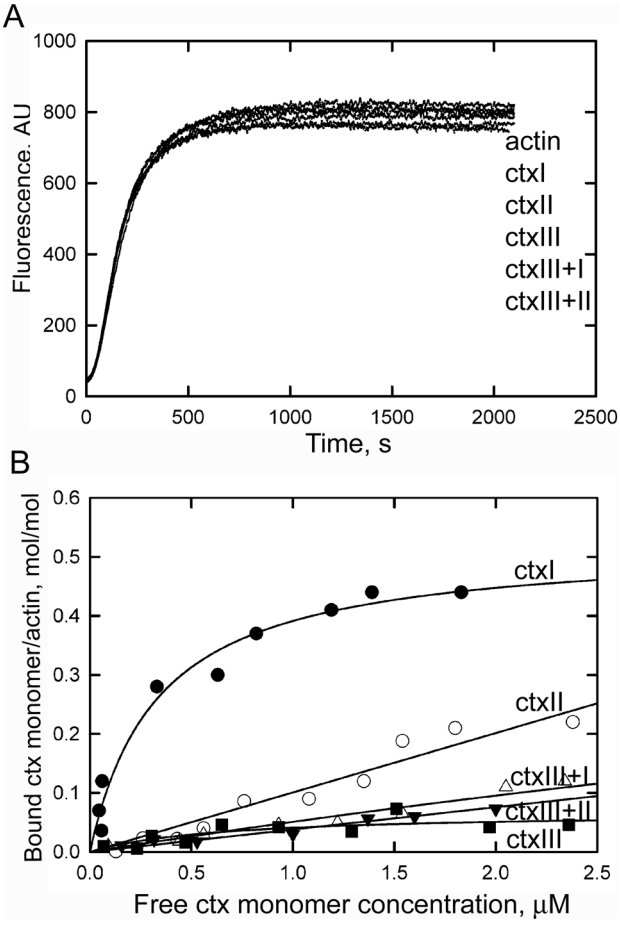


FIGURE 2: Interactions of recombinant cortexillins with actin. (A) Cortexillins do not affect actin polymerization. G-actin (6 μM) containing 10% pyrene actin was polymerized in 50 mM NaCl and 1 mM $MgCl_2$ with and without addition of cortexillins (1 μM), and polymerization at room temperature was monitored by the increase in pyrene fluorescence. Actin and cortexillin concentrations are given as monomers, although the actin was filamentous and, except for ctxIII, the cortexillins are dimers. AU, arbitrary units. (B) Binding of cortexillins to F-actin. Cortexillins (0.2–4 μM) free of any aggregates were mixed with G-actin (4 μM) in a solution containing 10 mM Tris, pH 7.0, 0.1 mM $CaCl_2$, 50 mM NaCl, 2 mM $MgCl_2$ and 0.1 mM ATP, incubated at room temperature for 2 h, and centrifuged at 120,000 rpm for 30 min at 4°C, and the supernatants and pellets were analyzed by SDS–PAGE for actin and cortexillin. As expected from results in A, the pellets of all of the samples contained the same amount of F-actin.

the composition of the gel-filtration peak in Figure 4E is consistent with the composition of the immunoprecipitate of FLAG-ctxIII on anti-FLAG magnetic beads (Table 2). Based on the properties of recombinant ctxIII in vitro, the gel filtration peak probably contained three components: a complex of DGAP1 and a FLAG-ctxIII/ctxI heterodimer, a complex of DGAP1 and a FLAG-ctxIII/ctxII heterodimer, and cdcD.

To confirm that cdcD is a contaminant and not a component of a ctxIII complex, we fractionated a lysate of ctxIII$^-$ cells not expressing FLAG-ctxIII on the FLAG-affinity column and analyzed the FLAG-peptide eluate by SDS–PAGE and HPLC-gel filtration (Figure 4G). SDS–PAGE of the FLAG-peptide eluate showed a single major band corresponding in position to cdcD (Figure 4G, inset), and HPLC gel filtration of the FLAG-peptide eluate revealed a major peak (Figure 4G) eluting at the same position (when compared with standards) as the major peak in the complex in Figure 4E. The elution time of cdcD was not unexpected because native cdcD has been shown to be a hexamer of the 88.5-kDa monomer (Arhzaouy *et al.*, 2012). The smaller peak in Figure 4G was a mixture of unidentified molecules of mass ~16 kDa. We concluded that cdcD in the HPLC peak of the affinity-purified FLAG-ctxIII complexes was a contaminant resulting from nonspecific binding of cdcD to the anti-FLAG antibody (even though cdcD does not contain a sequence similar to the sequence of FLAG peptide) and coelution of a cdcD hexamer and the FLAG-ctxIII complexes on gel filtration.

### Formation of a cortexillin III complex in vivo requires cortexillin I or cortexillin II

To determine whether formation of the ctxIII complexes required the presence of ctxI and/or ctxII, we expressed GFP-ctxIII in ctxI$^-$, ctxII$^-$, and ctxI$^-$II$^-$ cells and immunoprecipitated cell lysates on anti-GFP magnetic beads. Coomassie blue staining (Figure 5A) and immunoblots (Figure 5, B and C) of SDS–PAGE gels of the immunoprecipitates showed that GFP-ctxIII was immunoprecipitated from lysates of all three cells, ctxI was coimmunoprecipitated from lysates of ctxII$^-$ cells, ctxII was coimmunoprecipitated from lysates of ctxI$^-$ cells, and, of course, neither ctxI nor ctxII was coimmunoprecipitated from lysates of the ctxI$^-$II$^-$ cells. Of importance, there was no band corresponding to DGAP1 on the SDS–PAGE of the immunoprecipitate of GFP-ctxIII from lysates of the ctxI$^-$II$^-$ cells, that is, ctxIII did not bind to DGAP1 in the absence of both ctxI and ctxII (Figure 5A).

To investigate further the likelihood that ctxIII binds to DGAP1 only as heterodimers with ctxI or ctxII, we expressed GFP-ctxIII in DGAP1$^-$ cells and ctxIII$^-$ cells (Figure 5D) and immunoprecipitated it from cell lysates (Figure 5E). Both ctxI and ctxII coimmunoprecipitated with GFP-ctxIII expressed in DGAP1$^-$ cells, similar to their coimmunoprecipitation with GFP-ctxIII expressed in ctxIII$^-$ cells

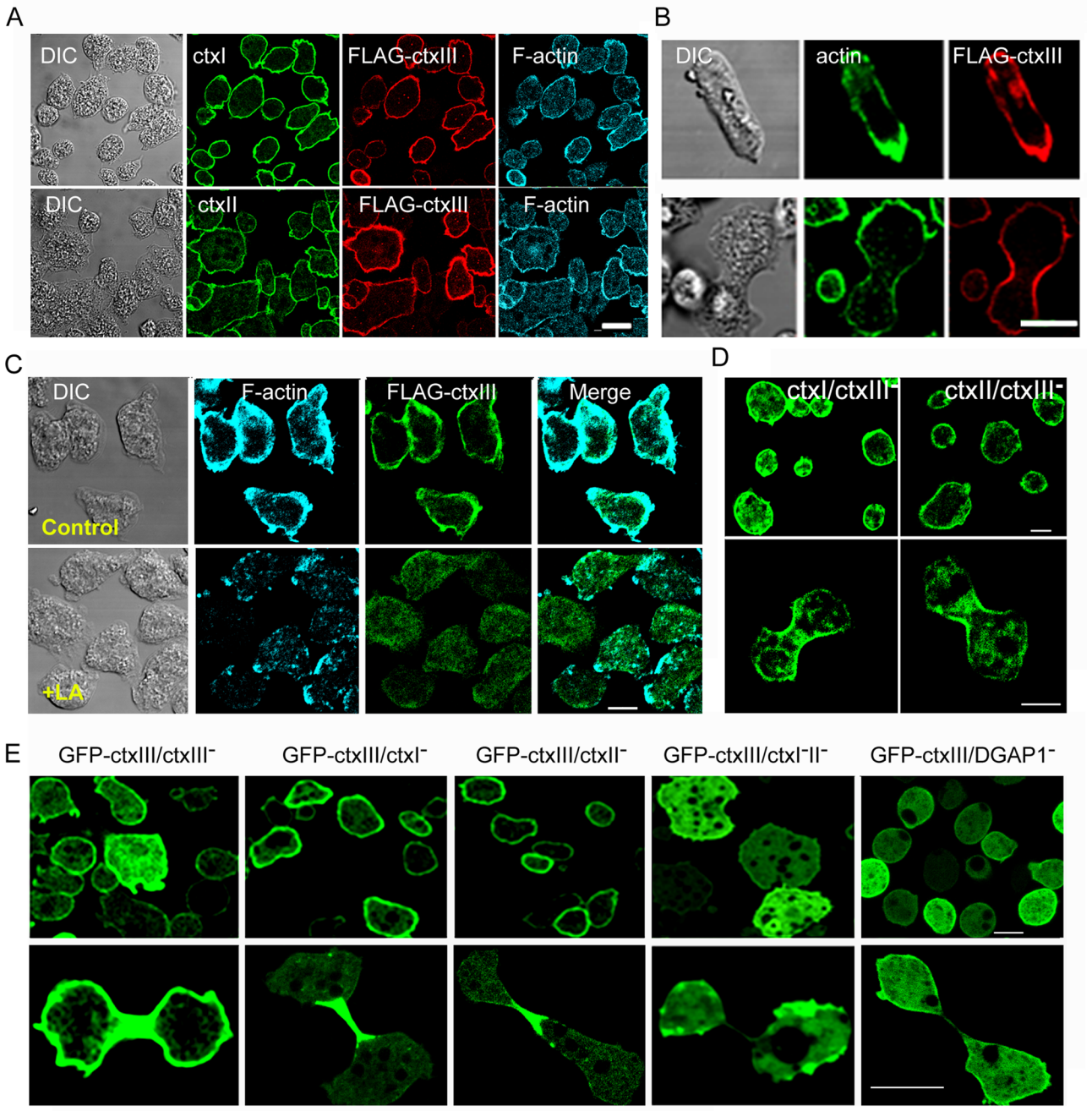


FIGURE 3: Localization of cortexillins and actin in vegetative, chemotaxing, and dividing cells by immunofluorescence. (A) Expressed FLAG-ctxIII (red) colocalized at the cortex of WT-cells with endogenous ctxI (top, green), endogenous ctxII (bottom, green), and F-actin (blue). (B) Expressed FLAG-ctxIII (red) colocalized with F-actin (green) at the front of motile cells (top) and the cleavage furrow of dividing cells (bottom). (C) Expressed FLAG-ctxIII (green) was diffuse in cells when actin filaments (blue) were depolymerized by addition of 4 μM latrunculin A (LA) for 5 min (bottom). (D) Endogenous cortexillins I and II (visualized by anti-ctxI and anti-ctxII antibody, respectively) localized to the cortex of vegetative cells (top) and the cleavage furrow of dividing ctxIII$^-$ cells (bottom). (E) Live images of GFP-ctxIII expressed in ctxI$^-$, ctxII$^-$, ctxIII$^-$, ctxI$^-$II$^-$, and DGAP1$^-$cells. GFP-ctxIII localized to the cortex of vegetative and the cleavage furrow of dividing ctxI$^-$, ctxII$^-$, and ctxIII$^-$ cells. However, GFP-ctxIII was mostly diffuse in the cytoplasm of vegetative cells and did not localize to the cleavage furrow of dividing ctxI$^-$II$^-$ and DGAP1$^-$ cells. Scale bars, 5 μm.

(Figure 5E). Thus the results shown in Figure 5 provide strong evidence that ctxIII forms heterodimers with both ctxI and ctxII in vivo, as it does in vitro, and that ctxIII binds to DGAP1 only as a heterodimer with either ctxI or ctxII.

To determine which region of ctxIII might be involved in formation of the ctxIII-DGAP1 complexes, presumably as a heterodimer with ctxI or ctxII, we expressed FLAG-tagged N- and C-terminal segments of ctxIII (residues 1–309 and 310–489, respectively) in ctxIII$^-$ cells with expressed FLAG-GFP as a control (Figure 6A). SDS–PAGE (Figure 6, B–D) and MS/MS analysis (Table 3) of immunoprecipitates on anti-FLAG magnetic beads showed that DGAP1, ctxI, and ctxII were coimmunoprecipitated with the C-terminal segment

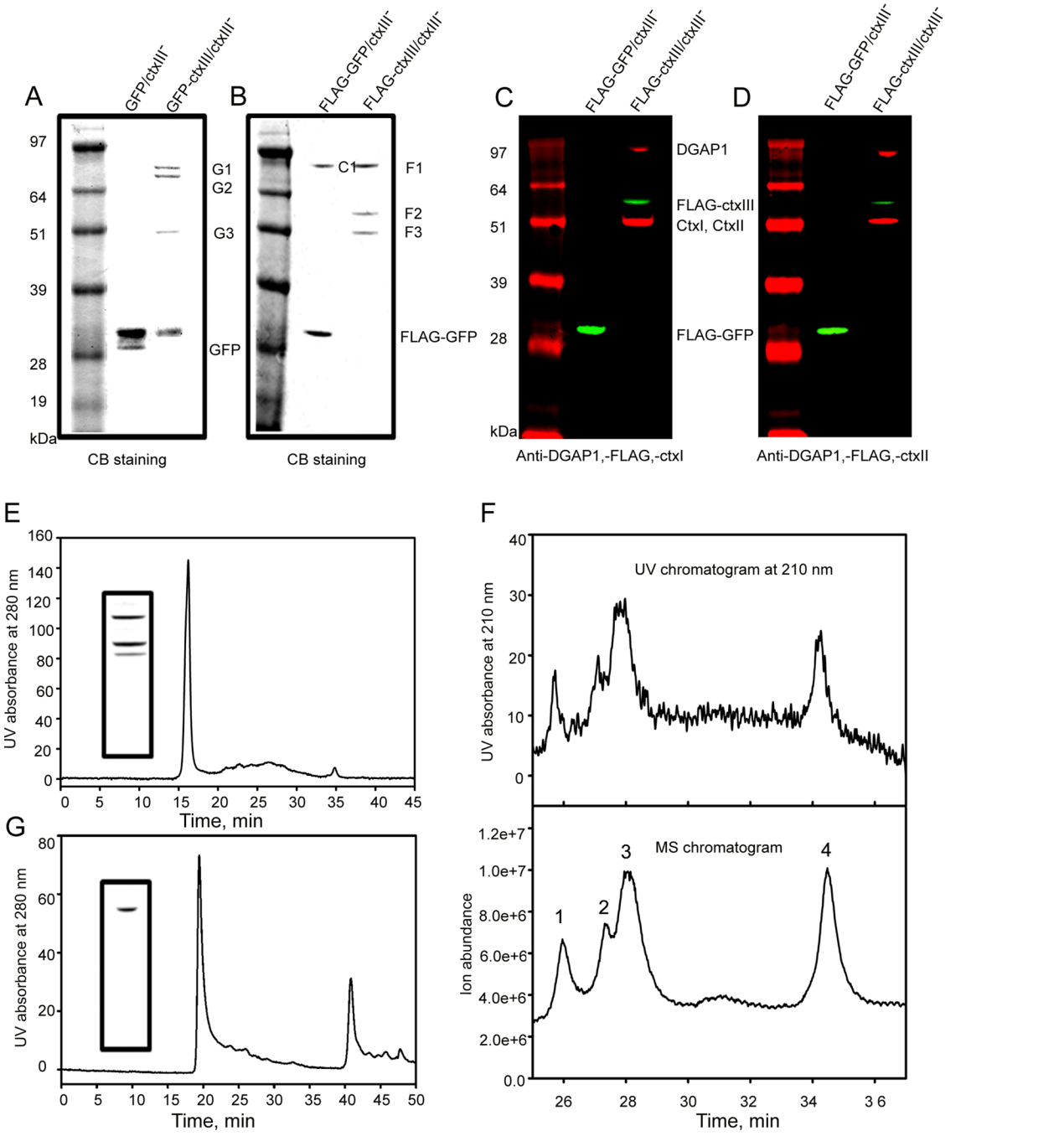


FIGURE 4: CtxIII expressed in ctxIII⁻ cells forms complexes with ctxI, ctxII, and DGAP1. (A, B) Coomassie blue–stained SDS–PAGE gels of proteins that immunoprecipitated with anti-GFP and anti-FLAG magnetic beads from lysates of cells expressing GFP-ctxIII or FLAG-ctxIII. Mass spectrometry (Table 2) identified G1 as DGAP1and F1 as DGAP1 and cdcD (cdcD was also present in control cells, C1, expressing FLAG-GFP); G2 and F2 as GFP-ctxIII and FLAG-ctxIII, respectively, and G3 and F3 as ctxI and ctxII, respectively. The band immediately above GFP in A is an unidentified contaminant also present in the control cells expressing GFP. (C, D) Western blots of SDS–PAGE gels of the same samples shown in A and B; anti-FLAG, green, and anti-DGAP1, anti-ctxI, and anti-ctxII, red. (E) HPLC gel-filtration chromatography of FLAG-ctxIII complexes purified by FLAG-affinity chromatography of a lysate of cells expressing FLAG-ctxIII. The elution time of the single major peak corresponded to a mass of a globular protein of ~600 kDa compared with standards chromatographed on the same column. Inset, Coomassie blue–stained SDS–PAGE gel of the sample that was applied to the HPLC column. (F) Reverse-phase chromatography of the peak fraction from HPLC gel filtration. Four peaks were identified by ultraviolet absorption (top) and MS (bottom) containing five proteins: peak 1, ctxI, 50,503 Da, calculated mass 50,505; peak 2, ctxII, 50,374 Da, calculated mass 50,460; peak 3, FLAG-ctxIII, 57,564 Da, calculated mass 57,506, and cdcD, 88,484 Da, calculated mass 88,554; and peak 4, DGAP1, 95,208 Da, calculated mass 94,925. (G) HPLC gel filtration of proteins isolated by FLAG-affinity chromatography of lysate of control ctxIII⁻ cells. Inset, Coomassie blue–stained SDS–PAGE gels of fraction analyzed. The major peak eluted at a time equivalent to a globular protein of mass ~660 kDa compared with protein standards on the same column.

| Band | Gene ID | Protein | Total peptides | Unique peptides | Coverage (%) |
|---|---|---|---|---|---|
| G1 | DDB0191437 | DGAP1 | 37 | 37 | 53 |
| G2 | DDB0232236 | GFP-ctxIII | 30 | 30 | 71 |
| G3 | DDB0191103 | ctxI | 16 | 14 | 39 |
| | DDB0185031 | ctxII | 28 | 26 | 64 |
| C1 | DDB0191154 | cdcD | 42 | 42 | 64 |
| F1 | DDB0191154 | cdcD | 42 | 42 | 59 |
| | DDB0191437 | DGAP1 | 41 | 41 | 55 |
| F2 | DDB0232236 | FLAG-ctxIII | 28 | 28 | 61 |
| F3 | DDB0191103 | ctxI | 21 | 20 | 43 |
| | DDB0185031 | ctxII | 17 | 16 | 43 |

Bands are identified as in Figure 3C. G1–G3, from ctxIII⁻ cells expressing GFP-ctxIII; C1, from control ctxIII⁻ cells; F1–F3, from ctxIII⁻ cells expressing FLAG-ctxIII. Total peptides do not include redundant sequences due to incomplete tryptic cleavage or covalent modification such as methionine oxidation.

TABLE 2: Proteins identified by mass spectrometry of tryptic peptides of proteins that coimmunoprecipitated with expressed GFP-ctxIII and FLAG-ctxIII.

of ctxIII but not with the N-terminal segment of ctxIII, presumably because the C-terminal segment can form a coiled-coil dimer with ctxI and II and the N-terminal segment cannot.

## Phenotype of cortexillin III–null cells

CtxIII⁻ cells grew more rapidly than WT cells both in suspension cultures (Figure 7A) and on bacterial lawns (Figure 7, B and C); the

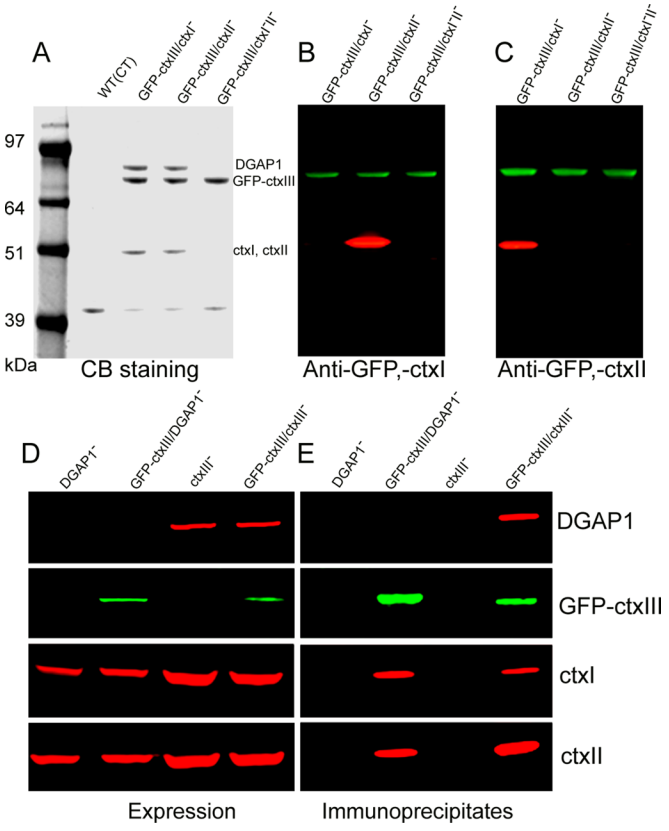


FIGURE 5: Expressed GFP-ctxIII binds to DGAP1 in vivo as a heterodimer with ctxI and ctxII. (A) Coomassie blue–stained and (B, C) immunoblots of proteins immunoprecipitated on anti-GFP magnetic beads from lysates of ctxI⁻, ctxII⁻, and ctxI⁻II⁻ cells expressing GFP-ctxIII; green, GFP; red, ctxI and ctxII. (D) Immunoblots of total lysates of DGAP1⁻ and ctxIII⁻ cells and the same cells expressing GFP-ctxIII. (E) Immunoblots of proteins immunoprecipitated on anti-GFP magnetic beads from lysates of DGAP1⁻ and ctxIII⁻ cells and the same cells expressing GFP-ctxIII.

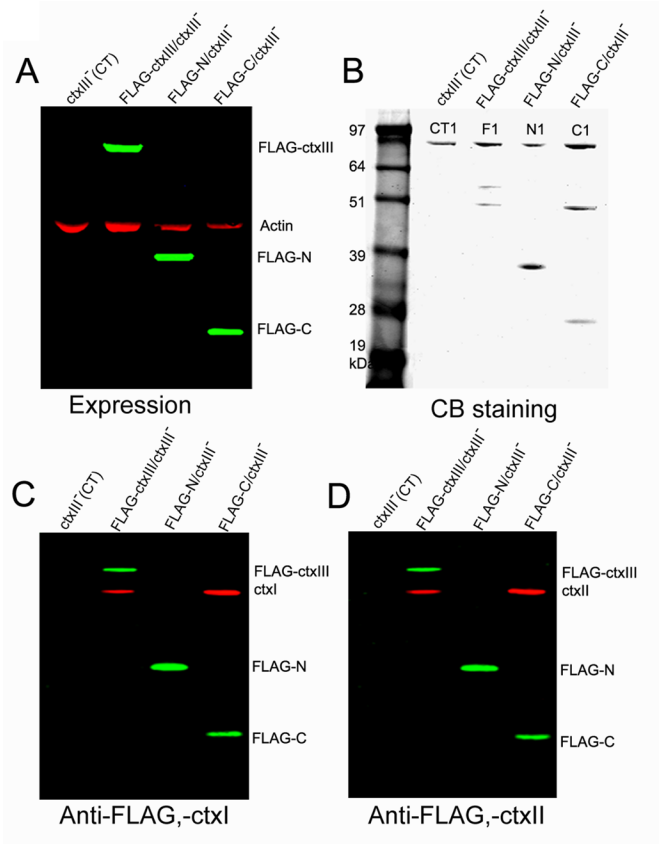


FIGURE 6: The C-terminus of ctxIII binds to cortexillin–DGAP1 complexes. (A) Immunoblot of SDS–PAGE gel of total cell lysates of ctxIII⁻ cells expressing FLAG-tagged full-length ctxIII, N-terminus of ctxIII (N), or C-terminus of ctxIII (C). (B) Coomassie blue–stained SDS–PAGE of proteins immunoprecipitated on anti-FLAG magnetic beads. As shown by MS (Table 3), all four bands at ~97 kDa contained the contaminating protein cdcD, but only the ~97-kDa bands in F1 and C1 contained DGAP1. (C, D) Immunoblots of the gel in B showing FLAG-tagged proteins (green) and ctxI and ctxII (red in C and D, respectively).

| Band | Gene ID | Protein | Total peptides | Unique peptides | Coverage (%) |
|---|---|---|---|---|---|
| CT1 | DDB0191154 | cdcD | 39 | 39 | 54 |
| F1 | DDB0191154 | cdcD | 47 | 47 | 64 |
| | DDB0191437 | DGAP1 | 30 | 30 | 40 |
| N1 | DDB0191154 | cdcD | 42 | 42 | 57 |
| C1 | DDB0191154 | cdcD | 36 | 36 | 51 |
| | DDB0191437 | DGAP1 | 30 | 30 | 40 |

The proteins of ~97 kDa in the SDS–PAGE gel shown in Figure 6B were identified by MS/MS of tryptic peptides. CT, control cells; F1, cells expressing FLAG-ctxIII; N1, cells expressing FLAG–N-terminal domain; C1, cells expressing FLAG–C-terminal domain.

**TABLE 3: Proteins identified by mass spectrometry of tryptic peptides of ~97-kDa proteins that coimmunoprecipitated with expressed FLAG–N-terminal and FLAG–C-terminal domains of ctxIII.**

doubling times in suspension culture were 13.1 h for WT cells and 11.3 h for ctxIII$^-$ cells. Phagocytosis (Figure 7D) and pinocytosis (Figure 7E) were also enhanced in ctxIII$^-$ cells. In contrast to Lee *et al.* (2010), we found that individual ctxIII$^-$ cells chemotaxed normally in a cAMP gradient (Figure 8A and Supplemental Videos S1 and S2). The speeds of WT cells and ctxIII$^-$ cells were 10.27 ± 1.35 and 10.13 ± 1.85 μm/min, respectively. In developmental buffer, starved ctxIII$^-$ cells initially formed normal streams (Figure 8B, top, and Supplemental Videos S3 and S4), but the streams tended to break up late in the process, resulting in smaller mounds than WT cells (Figure 8B, bottom) and smaller, but otherwise seemingly normal, fruiting bodies when cells were plated in developmental buffer on agar (Figure 8C). cAMP-wave analysis showed that the period between waves was 4.4 min for ctxIII$^-$ cells, shorter than the 6.2-min interval for WT cells (Supplemental Video S5).

## DISCUSSION

We found that purified recombinant ctxIII is an unstable monomer forming few, if any, homodimers, in contrast to recombinant ctxI and ctxII, both of which were dimers. This is consistent with the C-terminal sequence of ctxIII having lower predicted potential to form a coiled-coil helix than the C-terminal sequences of ctxI and ctxII. Of importance, ctxIII formed heterodimers when coexpressed with ctxI or ctxII. Recombinant ctxII and ctxIII and recombinant heterodimers of ctxIII with ctxI or ctxII had much lower affinity than recombinant ctxI for F-actin, and none of the recombinant proteins had any effect on the rate or extent of actin polymerization.

In vivo, as shown by coimmunoprecipitation, DGAP1, but not GAPA, bound to both expressed GFP-ctxIII and expressed FLAG-ctxIII. However, the association of ctxIII with DGAP1 required the presence of either ctxI or ctxII, strongly indicative that ctxIII binds to DGAP1 only as a heterodimer with either ctxI or ctxII. Heterodimerization of ctxIII with ctxI and ctxII in vivo is entirely consistent with heterodimerization of the recombinant proteins in vitro. Heterodimerization of the cortexillins in vivo is independent of DGAP1, as both ctxI and ctxII coimmunoprecipitated with ctxIII expressed in DGAP1$^-$ cells. Relevant to our observation of heterodimerization of ctxIII with both ctxI and ctxII, Faix *et al.* (2001) showed that ctxI and ctxII can heterodimerize both in vitro and in vivo. Because of the very low affinity of recombinant heterodimers with F-actin in vitro, one might ask whether the colocalization of cortexillins with F-actin in vivo is mediated by other proteins. Consistent with this speculation, ctxIII heterodimers colocalized with F-actin in vivo only as a complex with DGAP1.

Our data are consistent with and extend the observation of Lee *et al.* (2010) that ctxIII coimmunoprecipitates with DGAP1 but not with GAPA. However, there are two apparent differences between our results and previously published results. Most of the earlier experiments showed that the cortexillins, including ctxIII (Lee *et al.*, 2010), coimmunoprecipitated with both expressed Rac and expressed DGAP1, whereas in our experiments, DGAP1 but not Rac coimmunoprecipitated with expressed ctxIII. Second, we found that ctxII and DGAP1 coimmunoprecipitated with expressed ctxIII from lysates of ctxI$^-$ cells, although DGAP1 did not immunoprecipitate with ctxIII in the absence of ctxI and ctxII, and Faix *et al.* (2001) reported that DGAP1 did not immunoprecipitate with expressed ctxII in ctxI$^-$ cells. However, Faix *et al.* (2001) did observe DGAP1-dependent localization of ctxII to the cleavage furrow of dividing cells. Possibly both these differences can be explained by differences in the overexpressed proteins that were immunoprecipitated.

Why three cortexillins? In our previous study of cortexillins I and II (Shu *et al.*, 2012), we found that the single knockout of either ctxI or ctxII had little effect on cell phenotype, but that the double knockout of ctxI and ctxII had a strong phenotype. To the extent that similar parameters were investigated, the phenotype of the ctxI$^-$II$^-$ cells is quite different from the phenotype we report here for the ctxIII$^-$ cells. In assays of cAMP-induced chemotaxis, 35% fewer ctxI$^-$II$^-$ cells than WT cells were motile, and the motile cells moved 30% more slowly and with less directionality and more directional changes than WT cells (Shu *et al.*, 2012), whereas we now report no significant difference between cAMP-induced chemotaxis of ctxIII$^-$ cells and WT cells. Similarly, streaming is substantially delayed in ctxI$^-$II$^-$ cells (Shu *et al.*, 2012) but not in ctxIII$^-$ cells (our results), and whereas both cytokinesis and growth are severely impaired in ctxI$^-$II$^-$ cells (Shu *et al.*, 2012), both are enhanced in ctxIII$^-$ cells (our results). Thus ctxI and ctxII would seem to be positive regulators of cell division, growth, and chemotaxis, whereas ctxIII would appear to be a negative regulator of cytokinesis and growth, as well as endocytosis, which was not assayed in our previous study of ctxI$^-$II$^-$ cells. This brief summary suggests that these several processes are regulated by a balance of the interactions of different heterodimers of ctxI, ctxII, and ctxIII with the actin cytoskeleton. Of interest, as with our results with deletion of ctxIII, Faix and Dittrich (1996) found that deletion of DGAP1 increased the growth rate of amoebae growing on a bacterial lawn. This was later shown to be due to an increased rate of cell motility (Faix *et al.*, 1998).

In conclusion, it is attractive to imagine that variable interactions among the several proteins in the cortexillin complexes would allow different precise biological properties for different functional requirements, perhaps by allosteric conformational variations of the same proteins in different complexes. However, proof of different multiprotein complexes will depend on quantitative stoichiometric studies of the interactions of purified proteins in vitro and on the isolation and purification of cellular complexes of definitive

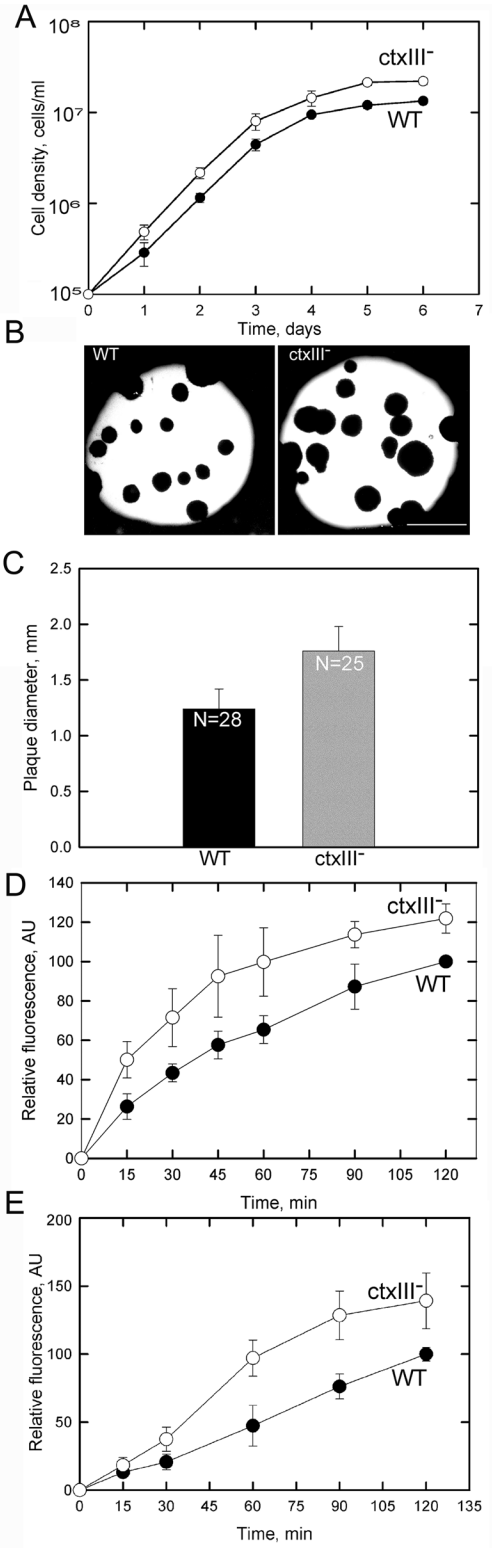


FIGURE 7: CtxIII is a negative regulator of cell growth and endocytosis. (A) CtxIII⁻ cells grew more rapidly than WT cells in suspension culture with doubling times of 11.3 vs. 13.1 h for ctxIII⁻ cells and WT cells, respectively. (B) CtxIII⁻ cells formed larger plaques than WT cells when grown on dead *K. aerogenes*. Bar, 5 mm. (C) Quantification of plaque size. (D, E) CtxIII⁻ cells phagocytosed fluorescein-labeled yeast (D) and pinocytosed rhodamine-labeled dextran (E) more rapidly than WT cells. Each data point in A, D, and E is the mean ± the SD from three separate experiments. Curves were fitted by regression analysis using Prism for Windows, version 6 (GraphPad, La Jolla, CA). The WT and ctxIII⁻ lines are significantly different with $p < 0.0001$. In C, *N* is the number of plaques counted in three independent experiments, and the error bars indicate the SD as determined by the two-tailed *t* test; WT and ctxIII⁻ are significantly different with $p < 0.005$.

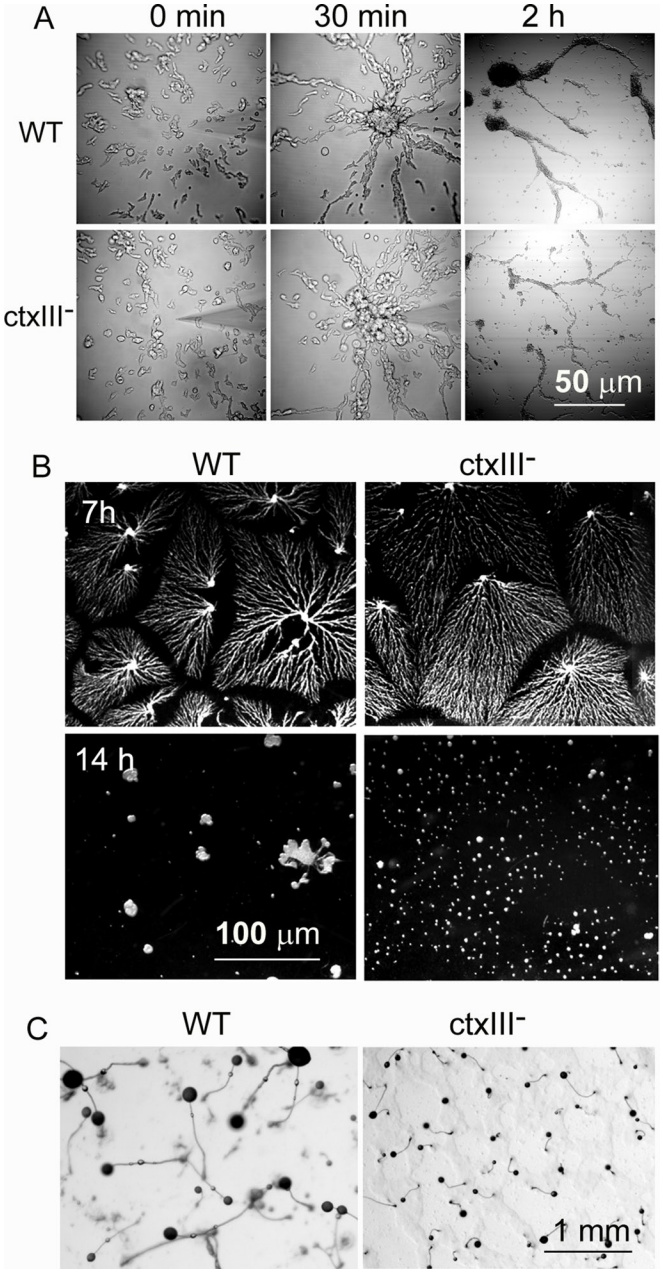


FIGURE 8: Deletion of ctxIII affects cell streaming and development. (A) Individual ctxIII⁻ cells chemotaxed normally toward a micropipette containing cAMP, but streams broke up by 2 h (see Supplemental Videos S1 and S2). (B) Starved WT and ctxIII⁻ cells both formed streams by 7 h and mounds by 14 h, but the streams of the ctxIII⁻ cells were looser, and the mounds were smaller (see Supplemental Videos S3 and S4). (C) Like WT cells, ctxIII⁻ cells in developmental buffer on agarose formed mounds by 24 h, but the mounds were much smaller than those formed by WT cells. All the experiments in A–C were done at least three times.

compositions from WT and mutant cells. Such experiments might be facilitated by initial isolation of the cortexillin complexes by immuno-affinity chromatography, as in Figure 4E, rather than by immunoprecipitation.

## MATERIALS AND METHODS

### Cloning and expression of cortexillin III

Genomic DNA was prepared using a genomic DNA purification kit (Promega, Madison, WI). ctxIII DNA was amplified and pieced together through PCR, subcloned onto pBluescript, and the sequence confirmed. The DNAs of N-terminal FLAG-tagged (DYKDDDDKENLYFQG-) full-length ctxIII, N-terminal-ctxIII (residues 1–309) and C-terminal-ctxIII (residues 310–489) were cloned to the pTIKL expression vector. N-terminal GFP-tagged full-length ctxIII was cloned to the DM317 vector for expression of the proteins in *Dictyostelium*. FLAG-ctxIII was also cloned into pFaxtBac1 for expression in SF-9 cells. N-terminal His-tagged (MRGSHHHHHHIPIEGR-) ctxI and ctxII (generous gifts of Jan Faix, Hannover Medical School, Hannover, Germany) and FLAG-ctxIII were cloned into pETDuet-1 (Novagen, Madison, WI) for bicistonic expression in Arctic Express (DE3)–competent *E. coli* (Agilent, Palo Alto, CA).

### Cell lines, culture, and transformation

*Dictyostelium* wild-type strain KAX3 and single- and double-knockout cells (ctxI$^-$, ctxII$^-$, ctxIII$^-$, ctxI$^-$II$^-$, and DGAP1$^-$) were grown in HL-5 liquid medium (HLG0101; Formedium, Hunstanton, UK). Expression plasmids FLAG-ctxIII, GFP-ctxIII, and FLAG- and GFP-N-terminal-ctxIII, FLAG- and GFP-C-terminal-ctxIII, GFP-ctxI, and GFP-ctxII were introduced into WT, ctxIII$^-$, ctxI$^-$, ctxII$^-$, ctxI$^-$ctxII$^-$, and DGAP1$^-$ cells using a gene pulser electroporator (Bio-Rad, Hercules, CA; Egelhoff *et al.*, 1991). Cells transformed with cDNAs were selected and maintained in HL-5 medium containing 16 µg/ml G418. Cells doubly transformed with GFP-ctxIII and Lifeact (Riedl *et al.*, 2008) were selected with 0.1 mg/ml hygromycin B in addition to G418. Recombined FLAG ctxIII cDNA was subcloned onto pFastBac4.5 vector (Invitrogen, Carlsbad, CA) and infected into SF-9 cells grown according to instructions provided by Invitrogen.

### Purification of recombinant cortexillins

*Dictyostelium* cells expressing FLAG-cortexillin III were lysed in 20 mM Tris, pH 7.4, 200 mM NaCl, 0.4% Triton X-100, protease inhibitors tablet (Roche), 1 tablet/50 ml, and 1 mM phenylmethylsulfonyl fluoride. Recombinant ctxIII was purified as described in Liu *et al.* (2010). SF-9 cells were broken by a French press in the foregoing buffer without Triton X-100. The lysate was centrifuged at 40,000 rpm in a Beckman 4.5 Ti rotor for 1 h at 4°C. The supernatant was mixed with 2–3 ml of equilibrated FLAG-resin (Sigma-Aldrich, St. Louis, MO) and thoroughly washed with lysis buffer without Triton. Cortexillin was eluted with 0.1 mg/ml FLAG-peptide in the washing buffer. Bacteria were lysed by the same procedure as for Sf-9 cells, and His-ctxI and His-ctxII were purified from the supernatant fraction by chromatography on Ni-NTA-agarose (Qiagen, Hilden, Germany) as recommended by the manufacturer. Coexpressed FLAG-ctxIII and His-ctxI or His-ctxII were purified from the bacterial lysate by sequential chromatography on a FLAG-affinity column and a Ni-NTA-agarose column. Protein concentrations were determined by the Bradford method with bovine serum albumin as a standard.

### Actin preparation, binding, and polymerization assays

Rabbit muscle acetone powder was purchased from PelFreez (Rogers, AR), and actin was prepared as described (Spudich and Watt, 1971). For the actin-binding assay, actin was dialyzed against 10 mM Tris, pH 7.0, 0.1 mM ATP, and 0.1 mM $CaCl_2$ overnight and then centrifuged at 335,000 × *g* for 60 min at 4°C in a Beckman TL-100 centrifuge. Cortexillins were dialyzed against 300 mM NaCl and 10 mM Tris, pH 7.0, and centrifuged at 120,000 × *g* for 30 min in the same centrifuge.

Actin polymerization assays were performed as described (Liu *et al.*, 2010). G-actin, 6 µM, in G-buffer, 4 mM Tris, pH 7.4, 0.1 mM ATP, 0.1 mM $CaCl_2$, containing 10% pyrene-labeled actin (Cytoskeleton, Denver, CO), with and without 1 µM cortexillins, was polymerized by addition of $MgCl_2$ and NaCl to final concentrations of 2 and 100 mM, respectively. Polymerization at room temperature (21–22°C) was monitored by the increase in fluorescence in a LS55 luminescence spectrometer with emission wavelength of 406 nm, excitation wavelength of 365 nm, and slit width of 8 nm.

For actin-binding assays, the actin and cortexillin were mixed and $MgCl_2$ added to initiate actin polymerization. Final concentrations were 4 µM actin and 0.2–4 µM cortexillin in the actin buffer containing 50 mM NaCl and 2 mM $MgCl_2$. After incubation for 2 h at room temperature for actin polymerization, the mixture was centrifuged at 120,000 × *g* for 30 min at 10°C in the same centrifuge to pellet the F-actin, and the cortexillins in the supernatant and pellet were quantified by SDS–PAGE.

### Cell growth, phagocytosis, and pinocytosis

Cell growth in suspension culture was measured as described (Shu *et al.*, 2010). Briefly, 50 ml of cells ($1 \times 10^5$ cells/ml) was cultured in a 250-ml flask on a rotary shaker at 145 rpm. Cells were counted daily using a cellometer (AutoT4 cell counter; Nexcelom Bioscience). Plaque expansion assays were performed as described (Shu *et al.*, 2005). A mixture of *Dictyostelium* amoebae and heat-killed *Klebsiella aerogenes* was seeded onto Millipore (Bedford, MA) black filters on pads in Petri dishes, and plaque sizes were measured after 5 d. Phagocytosis and pinocytosis assays were performed as described (Maniak *et al.*, 1995; Shu *et al.*, 2010) with some modifications. For phagocytosis, cells were suspended at $5 \times 10^6$/ml in Sorenson's buffer, 17 mM potassium phosphate, pH 6.1, and tetramethylrhodamine isothiocyanate (TRITC)–yeast was added at a yeast:cell ratio of 5:1. For pinocytosis, cells were suspended in HL-5 medium at $5 \times 10^6$/ml, and TRITC-dextran was added to a final concentration of 2 mg/ml. In both the phagocytosis and pinocytosis assays,1-ml samples were transferred at the indicated times to microtubes containing 100 µl of 0.4% trypan blue to quench background fluorescence, and the suspensions were centrifuged. The cell pellets were washed and resuspended in 1 ml of Sorenson's buffer, and fluorescence was measured in a LS55 luminescence spectrometer with excitation wavelength of 544 nm and emission wavelength of 577 nm. All experiments were repeated at least three times. All experiments were carried out at room temperature, 21–22°C.

### Cell streaming and development

Self-streaming and development assays were performed as described by Shu *et al.* (2012). Briefly, $1.5 \times 10^7$ cells were harvested, resuspended at $5 \times 10^5$ cells/ml, plated on 60-mm Petri dishes, and allowed to adhere for 30 min. The cells were washed twice with starvation buffer (20 mM 2-(*N*-morpholino)ethanesulfonic acid, pH 6.8, 0.2 mM $CaCl_2$, 2 mM $MgSO_4$). Images of self-streaming cells were taken every minute with a Discovery V12 stereomicroscope (Carl Zeiss) equipped with a PlanApo 1.0× objective and an AxioCam camera automated by AxioVision 4 software. Development was monitored for 24 h in developmental buffer, 5 mM $Na_2HPO_4$, 5 mM

$KH_2PO_4$, pH 6.2, 0.2 mM $CaCl_2$, and 2 mm $MgSO_4$ on agarose plates, and for 5 d after, cells were spotted on a bacterial lawn (Shu *et al.*, 2010). Results were recorded with the same stereomicroscope system that was used to visualize self-streaming. All experiments were performed at least three times at room temperature, 21–22°C.

### Fluorescence microscopy and chemotaxis assay

Fluorescence microscopy was performed as described (Shu *et al.*, 2012). For immunolocalization, cells were fixed with 1% formaldehyde, 0.1% glutaraldehyde, and 0.01% Triton X-100 in phosphate buffer (5 mM $Na_2HPO_4$, 5 mM $KH_2PO_4$, pH 6.2) at room temperature for 15 min, washed with phosphate buffer, and incubated with one or more of the following antibodies for 60 min at 37°C: rabbit anti-actin (Sigma-Aldrich) diluted 100-fold, monoclonal mouse anti-FLAG M2 (Sigma-Aldrich) diluted 700-fold, rabbit anti-FLAG antibody (Sigma-Aldrich), or monoclonal mouse anti–cortexillin I or anti–cortexillin II (Developmental Studies Hybridoma Bank, Iowa City, IA) without dilution in phosphate buffer supplemented with 1% bovine serum albumin and 0.2% saponin. F-actin was stained with rhodamine or Alexa Fluor 647–phalloidin (Molecular Probes, Eugene, OR). Cells were exposed to 4 µM latrunculin A for 5 min. Images were acquired with an LSM-510 laser scanning confocal fluorescence microscope (Carl Zeiss). For fluorescence microscopy of live cells, cells were placed on a chambered coverglass (Lab-Tek, NUNC, Rochester, NY) in phosphate buffer. Images were acquired at room temperature with an LSM -780 laser scanning confocal microscope (Carl Zeiss) equipped with a PLANapo 63× oil objective.

Micropipette assays of cAMP-induced *Dictyostelium* chemotaxis were performed as described (Parent *et al.*, 1998; Shu *et al.*, 2010). Aggregation-competent cells were suspended in phosphate buffer on a chambered coverslip. A chemoattractant gradient was generated with 1 µM cAMP in a micropipette. Chemotactic migration was continuously recorded at intervals of 10 s using an Axiovert 200 inverted microscope and AxioVision software (Carl Zeiss) and processed with MetaMorph software (Molecular Devices, Sunnyvale, CA). Cell speed, motility, and shape changes during chemotaxis were assayed by a two-dimensional dynamic image analysis system (Wessels *et al.*, 2007).

### Electrophoresis and immunoblotting

SDS–PAGE was performed by standard procedures on NUPAGE gels (Invitrogen, Carlsbad, CA). Cell lysates were subjected to SDS–PAGE analysis and transferred to membranes by iBlot gel transfer stack (Invitrogen). The membranes were blotted with rabbit anti-FLAG (Sigma-Aldrich) diluted 1:3000, ctxI or ctxII antibody (Developmental Studies Hybridoma Bank) diluted 1:10, mouse anti-GFP (Covance, Berkeley, CA), and/or mouse monoclonal DGAP1 antibody (gift from J. Faix) diluted 1:200. Secondary antibodies, goat IRDye800, anti-rabbit immunoglobulin G (IgG; Rockland Immunochemicals, Gilbertsville, PA), and Alexa Fluor 680 goat anti-mouse IgG (Molecular Probes, Invitrogen) were diluted 1:7000. Proteins were quantified with the Odyssey infrared imaging system (LI-COR Biosciences, Lincoln, NE).

### Coimmunoprecipitation

A total of $1 \times 10^7$ cells was harvested by low-speed centrifugation, washed twice with 20 mM Tris-HCl, pH 7.4, and resuspended in 1 ml of cold lysis buffer (150 mM NaCl, 50 mM Tris HCl, pH 8.0, and 0.6% Triton X-100 containing protease inhibitor cocktail tablets from Roche, Mannheim, Germany). The crude lysates were spun at 10,000 × g for 10 min at 4°C. Clear lysates were incubated at 4°C for 1 h with 100 µl of either anti-FLAG M2 magnetic beads (M8823; Sigma-Aldrich) or µMACS anti-GFP MicroBeads (Miltenyl Biotech, Bergisch, Germany). After binding, the anti-FLAG beads were washed four times with lysis buffer without Triton and eluted with 0.1 mg/ml of FLAG-peptide. After binding, the anti-GFP beads were separated by a µColumn on a magnetic separator, µMACS GFP isolation kit (130-091-125), according to the manufacturer's protocol. The beads were washed four times with buffer I (150 mM NaCl, 1% Igepal CA-630, 0.5% sodium deoxycholate, 0.1% SDS, 50 mM Tris HCl, pH 8.0) and twice with wash buffer II (20 mM Tris HCl, pH 7.5). Proteins were eluted by buffer containing 50 mM Tris HCl, pH 6.8, 50 mM dithiothreitol, 1% SDS, 1 mM EDTA, 0.005% bromophenol blue, and 10% glycerol. The proteins eluted from the anti-FLAG and anti-GFP beads were separated by SDS–PAGE, and the gels were either immune blotted or stained with Coomassie blue and excised for mass spectrometry analysis after in-gel trypsin digestion by a standard protocol.

### Analytical ultracentrifugation

The centrifugation experiments were performed in the ProteomeLab XL-I analytical ultracentrifuge (Beckman Coulter, Indianapolis, IN) using absorption optics and a detection wavelength of 280 nm. Purified proteins were dialyzed against 300 mM NaCl, 50 mM Tris, pH 7.4, overnight and centrifuged for 30 min at 50,000 rpm in a Beckman TL-100 centrifuge to remove any aggregates that might be present. Samples, 400 µl, were loaded into 12-mm-path-length AUC cells, with the dialysis buffer used as a reference. Samples were placed in the rotor and temperature equilibrated in the centrifuge under vacuum for 1 h after the set temperature of 20°C had been reached. The rotor was accelerated to 50,000 rpm, and scans were immediately started in a continuous mode and recorded until no further boundary movement was observed. Data were analyzed in terms of continuous $c(s)$ distributions using the SEDFIT program (Schuck, 2000), and the same software was used to calculate average molecular weights corresponding to the main peaks of the $c(s)$ distribution. Sedimentation coefficients distributions were corrected to standard conditions at 20°C in water, $S_{20,w}$.

### Gel-filtration and mass spectroscopy of native proteins

Gel filtration chromatography was performed on a TSK G300SB-C18 (7.5 × 600 mm, 10 µm, TOSOH) equilibrated with 50 mM Tris-HCl, 200 mM NaCl, pH 7.4. The column was connected to the Agilent 1100 series HPLC (Agilent, Santa Clara, CA) and eluted at a rate of 0.6 ml/min. Absorbance was read at 280 nm. The column was calibrated using the gel-filtration high–molecular weight kits (GE Healthcare Life Sciences, Little Chalfont, UK, and Sigma-Aldrich, St. Louis, MO). HPLC fractions were collected using the Agilent analytical fraction collector.

Selected fractions from the gel filtration column were concentrated by ultrafiltration ($M_r$ > 10,000; Centricon YM-10; Amicon) and applied to HPLC mass spectrometry for mass determination of intact proteins. Proteins were separated by reverse-phase HPLC (Agilent 1100 series HPLC; Agilent) with a Zorbax 300SB-C18 (2.1 × 50 mm, 3.5 µm; Agilent) and introduced into the mass spectrometer as described (Apffel *et al.*, 1995; Taggart *et al.*, 2000). Positive-ion electrospray ionization mass spectra for intact proteins were obtained with an Agilent 6224 mass spectrometer equipped with an ion electrospray ionization interface and a time-of-flight mass detector (Agilent). Mass spectra were analyzed and deconvoluted as described (Stevens *et al.*, 2009) using MassHunter, version B.04.00 (Agilent).

### Mass spectroscopy of tryptic peptides

Liquid chromatography–tandem mass spectrometry was performed using a nanoLC-Ultra 2D system (Eksigent, Dublin, CA) coupled to an Orbitrap Elite mass spectrometer (Thermo Scientific, San Jose, CA). The peptide sample was first loaded onto a Zorbax 300SB-C18 trap column (Agilent) and then separated on a reversed-phase Beta-Basic C18 PicoFrit analytical column (New Objective, Woburn, MA) using a linear gradient (buffer A: 0.1% formic acid in water; buffer B: 0.1% formic acid in acetonitrile). Eluted peptides were sprayed into the Orbitrap Elite equipped with a nanospray ionization source. Survey MS spectra were acquired in the Orbitrap, and data-dependent MS/MS scans were performed in the linear ion trap with dynamic exclusion.

For protein identification, raw data files generated from the Orbitrap Elite were analyzed using a Proteome Discoverer, version 1.4, software package (Thermo Scientific, Waltham, MA) and the Mascot search engine running on an eight-processor cluster at the National Institutes of Health (http://biospec.nih.gov, version 2.4). The following database search criteria were used: database, Sp-Trembl (SwissProt + Trembl); taxonomy, *Dictyostelium discoideum*; enzyme, trypsin; maximum missed cleavages, 2; variable modifications, oxidation, deamidation; fixed modifications, carbamidomethylation; peptide precursor mass tolerance, 25 ppm; MS/MS fragment mass tolerance, 0.8 Da. Peptide-spectrum matches were filtered to achieve an estimated false discovery rate of 1% based on a target-decoy database search strategy.

## ACKNOWLEDGMENTS

We thank Richard Firtel (University of California, San Diego, La Jolla, CA), Douglas Robinson (Johns Hopkins University, Baltimore, MD), Jan Faix (Hannover Medical School, Hannover, Germany), the Developmental Studies Hybridoma Bank (Iowa City, IA), and the Dictybase Stock Center (Northwestern University, Chicago, IL) for cell lines, DNA constructs, antibodies, and other reagents; Joseph Brzostowski (Laboratory of Immunogenetics Imaging Facility, National Institute of Allergy and Infectious Diseases) for the analysis of cAMP waves; and Xufeng Wu (National Heart, Lung, and Blood Institute Light Microscopy Core) for help in confocal microscopy. We also thank Jianshe Yan (National Institute of Allergy and Infectious Diseases) and Nathan Kung, Ikuko Fujiwara, Kevin Pridham, Maciej Olszewski, Alan Peterkofsky, and Rodney Levine (National Heart, Lung, and Blood Institute) for their generous assistance. We gratefully acknowledge insightful comments by Hanna Brzeska (National Heart, Lung, and Blood Institute). This research was supported by the Intramural Research Program of the National Heart, Lung, and Blood Institute, National Institutes of Health.

## REFERENCES

Apffel A, Fischer S, Goldberg G, Goodley PC, Kuhlmann FE (1995). Enhanced sensitivity for peptide mapping with electrospray liquid chromatography-mass spectrometry in the presence of signal suppression due to trifluoroacetic acid-containing mobile phases. J Chromatogr A 712, 77–190.

Arhzaouy K, Strucksberg KH, Tung SM, Tangavelou K, Stumpf M, Faix J, Schröder R, Clemen CS, Eichinger L (2012). Heteromeric p97/p97R155C complexes induce dominant negative changes in wild-type and autophagy 9-deficient *Dictyostelium* strains. PLoS One 7, 46879.

Castresana J, Saraste M (1995). Does Vav bind to F-actin through a CH domain? FEBS Lett 374, 149–151.

Dickinson DJ, Robinson DN, Nelson WJ, Weis WI (2012). α-Catenin and IQGAP regulate myosin localization to control epithelial tube morphogenesis in *Dictyostelium*. Dev Cell 23, 533–546.

Effler JC, Kee YS, Berj JM, Tran MN, Iglesias PA, Robinson DN (2006). Mitosis-specific mechanosensing and contractile protein redistribution control cell shape. Curr Biol 16, 1962–1967.

Egelhoff TT, Brown SS, Spudich JA (1991). Spatial and temporal control of nonmuscle myosin localization: identification of a domain that is necessary for myosin filament disassembly in vivo. J Cell Biol 112, 677–688.

Faix J, Clougherty C, Konzok A, Mintert U, Murphy J, Albrecht R, Mühlbauer, Robinsin J (1998). The IQGAP-related protein DGAP1 interacts with Rac and is involved in the modulation of the F-actin cytoskeleton and control of cell motility. J Cell Sci 111, 3059–3071.

Faix J, Dittrich W (1996). DGAP1, a homologue of rasGTPase activating proteins that controls growth, cytokinesis, and development in *Dictyostelium discoideum*. FEBS Lett 394, 251–257.

Faix J, Steinmetz M, Boves H, Kammerer RA, Lottspeich F, Mintert U, Murphy J, Stock A, Aebi U, Gerisch G (1996). Cortexillins, major determinants of cell shape and size, are actin-bundling proteins with a parallel coiled-coil tail. Cell 86, 631–642.

Faix J, Weber I, Mintert U, Köhler J, Lottspeich F, Marriott G (2001). Recruitment of cortexillin into the cleavage furrow is controlled by Rac1 and IQGAP-related proteins. EMBO J 20, 3705–3715.

Friedberg F, Rivero F (2010). Single and multiple CH (calponin homology) domain-containing multidomain proteins in *Dictyostelium disodium*: an inventory. Mol Biol Rep 37, 2853–2862.

Girard KD, Chaney C, Delannoy M, Kuo SC, Robinson DN (2004). Dynacortin contributes to cortical elasticity and helps define the shape change of cytokines. EMBO J 23, 1536–1546.

Kee YS, Ren Y, Dorfman D, Iijima M, Firtel R, Iglesias PA, Robinson DN (2012). A mechanosensory system governs myosin II accumulation in dividing cells. Mol Biol Cell 23, 1510–1523.

Lee S, Shen Z, Robinson DN, Briggs S, Firtel R (2010). Involvement of the cytoskeleton in controlling leading-edge function during chemotaxis. Mol Biol Cell 21, 1810–1824.

Liu X, Shu S, Hong MS, Yu B, Korn ED (2010). Mutation of actin Tyr-53 alters the conformations of the DNase I-binding loop and the nucleotide-binding cleft. J Biol Chem 285, 9729–9739.

Lupas A, Van Dyke M, Stock J (1991). Predicting coiled coils from protein sequences. Science 252, 1162–1164.

Maniak M, Rauchenberger R, Albrecht R, Murphy J, Gerisch G (1995). Coronin involved in phagocytosis: dynamics of particle-induced relocalization visualized by a green fluorescent protein tag. Cell 83, 915–924.

Mondal S, Burgute B, Rieger D, Müller R, Rivero F, Faix J, Schleicher M, Noegel AA (2010). Regulation of the actin cytoskeleton by an interaction of IQGAP related protein GAPA with filamin and cortexillin I. PLoS One 5, e15440.

Parent CA, Blacklock BJ, Froehlich WM, Murphy DB, Devreotes PN (1998). G protein signaling events are activated at the leading edge of chemotactic cells. Cell 95, 81–91.

Reichl EM, Ren Y, Morphew MK, Delannoy M, Effler JC, Girard KD, Divi S, Iglesias PA, Kuo SC, Robinson DN (2008). Interactions between myosin and actin crosslinkers control cytokinesis contractility dynamics and mechanics. Curr Biol 18, 471–480.

Ren Y, Effler JC, Norstrom M, Luo T, Firtel RA, Iglesias PA, Rock RS, Robinson DA (2009). Mechanosensing through cooperative interactions between myosin II and the actin crosslinker cortexillin I. Curr Biol 19, 1421–1428.

Riedl J *et al.* (2008). Lifeact: a versatile marker to visualize F-actin. Nat Methods 5, 605–607.

Schroth-Diez B, Gerwig S, Ecke M, Hegerl R, Diez S, Gerisch G (2009). Propagating waves separate two states of actin organization in living cells. HSFP J 3, 412–427.

Schuck P (2000). Size-distribution analysis of macromolecules by sedimentation velocity ultracentrifugation and Lamm equation modeling. Biophys J 78, 1606–1619.

Schuck P (2005). Diffusion-deconvoluted sedimentation coefficient distributions for the analysis of interacting and non-interacting protein mixtures. In: Analytical Ultracentrifugation, ed. DJ Scott, SE Harding, and AJ Rowe, Cambridge, UK: Royal Society of Chemistry, 26–50.

Shannon KB (2012). IQGAP family members in yeast, *Dictyostelium*, and mammalian cells. Int J Cell Biol 2012, 894817.

Shu S, Liu X, Korn ED (2005). Blebbistatin and blebbistatin-inactivated myosin II inhibit myosin II-independent processes. Proc Natl Acad Sci USA 102, 1472–1477.

Shu S, Liu X, Kriebel PW, Daniels MP, Korn ED (2012). Actin cross-linking proteins cortexillin I and II are required for cAMP signaling during *Dictyostelium* chemotaxis and development. Mol Biol Cell 23, 390–400.

Shu S, Liu X, Kriebel PW, Hong MS, Daniels MP, Parent CA, Korn ED (2010). Expression of Y53A-actin in *Dictyostelium* disrupts the cytoskeleton and

inhibits intracellular and extracellular chemotactic signaling. J Biol Chem 285, 27713–27725.
Simson R, Wallraff E, Faix J, Niewöhner J, Gerisch G, Sackmann E (1998). Membrane bending modulus and adhesion energy of wild-type and mutant cells of *Dictyostelium* lacking talin or cortexillins. Biophys J 74, 514–522.
Spudich JA, Watt S (1971). The regulation of rabbit skeletal muscle contraction. I. Biochemical studies of the interaction of the tropomyosin-troponin complex with actin and the proteolytic fragments of myosin. J Biol Chem 246, 4866–4871.
Steinmetz MO, Stock A, Schulthess T, Landwehr R, Lustig A, Faix J, Gerisch G, Aeba U, Kammerer RA (1998). A distinct 14 residue site triggers coiled-coil formation in cortexillin I. EMBO J 17, 1883–1891.
Stevens LA, Levine RL, Gochuico BR, Moss J (2009). ADP-ribosylation of human defensing HNP-1 results in the replacement of the modified arginine with the noncoded amino acid ornithine. Proc Natl Acad Sci USA 106, 19796–19800.
Stock A, Steinmetz MO, Janmey PA, Aebi U, Gerisch G, Kammerer RA, Weber I, Faix J (1999). Domain analysis of cortexillin I: actin-bundling, $PIP_2$-binding and the rescue of cytokinesis. EMBO J 18, 5274–5284.
Taggart C, Cervantes-Laurean D, Kim G, McElvaney NG, Wehr N, Moss J, Levine RL (2000). Oxidation of either methionine 351 or methionine 358 in alpha 1-antitrypsin causes loss of anti-neutrophil elastase activity. J Biol Chem 275, 27258–27265.
Weber I, Gerisch G, Heizer C, Murphy J, Badelt K, Stock A, Schwartz JM, Faix J (1999). Cytokinesis mediated through the recruitment of cortexillins into the cleavage furrow. EMBO J 18, 586–594.
Wessels D, Lusche DF, Kuhl S, Heid P, Soll DR (2007). PTEN plays a role in the suppression of lateral pseudopod formation during *Dictyostelium* motility and chemotaxis. J Cell Sci 120, 2517–2531.